Applied Surface Science 504 (2020) 144469

Contents lists available at ScienceDirect

Applied Surface Science

journal homepage: www.elsevier.com/locate/apsusc

Full Length Article

Equilibrium morphology evolution of FCC cobalt nanoparticle under CO and hydrogen environments

Mengting Yu[a,b], Lili Liu[a,b], Litao Jia[a,c], Debao Li[a,c], Qiang Wang[a,*], Bo Hou[a,*]

[a] State Key Laboratory of Coal Conversion, Institute of Coal Chemistry, Chinese Academy of Sciences, Taiyuan, Shanxi 030001, People's Republic of China
[b] University of Chinese Academy of Sciences, Beijing 100049, People's Republic of China
[c] Dalian National Laboratory for Clean Energy, Dalian 116023, People's Republic of China

ARTICLE INFO

Keywords:
Cobalt nanoparticle
CO environment
Hydrogen environment
Wulff construction
DFT

ABSTRACT

Metal nanoparticles could change their shape and exposed certain facet under specific reaction conditions, resulting in greatly influence the performance of catalysts in heterogeneous catalysis. Combining spin-polarized density functional theory and *ab initio* atomistic thermodynamics, the equilibrium morphology evolution of FCC cobalt nanoparticle had been investigated under CO and hydrogen environments. The phase diagram clearly revealed the stable coverage could be affected by temperature and CO and hydrogen partial pressure. According to the surface energies of four surfaces, Wulff construction was introduced to characterize the morphologies of the Co catalyst at diverse temperatures and pressures. At the typical temperature (675 K) of hydrogen reduction, the estimated surface proportion ratio of the Co(3 1 1) exposed the B5 site could exist a marked increase, which was also consistent with the available Co catalyst reduced under experimental conditions. Our results would give direct insights into the understanding and quantitative description of structure evolution as well as active facets of the Co nanoparticles under the realistic FTS reaction condition.

1. Introduction

Shape-controlled synthesis and crystal plane effect of metal nanoparticles are of great interest to the catalytic field because the activation of a nanomaterial can be improved by tuning the shape [1–7]. For these reasons, in the early 2000s, the relationships between the catalytic behavior of heterogeneous catalysts and morphology of nanomaterials have been a hot topic [8–13]. Generally, the catalytic properties of the high-surface-area nanocatalytic materials are also closely related to the exposed crystal facets [8,14]. In other words, the morphology of the catalyst particles determined by the exposed crystal planes could greatly influence the reactivity and/or the selectivity for heterogeneous catalysis reaction.

Recently, many studies had been reported that the synthesis of nanocrystals with various morphologies, and furtherly explored the facet dependent catalytic properties. Li *et al.* [15] investigated that the face-centered cubic (FCC) Ru catalysts exhibited higher activity than the hexagonal close-packed (HCP) Ru catalysts in the aqueous-phase Fischer-Tropsch Synthesis (FTS) due to the higher density of active sites of FCC Ru catalysts. Spencer *et al.* [16] observed that the Fe(1 1 1) surface could greatly increase the ammonia production rate. Experimentally with theoretical calculations, ceria nanorods had exhibited more active in comparison with nanoparticles for CO oxidation due to the higher reactivity of {0 0 1}/{1 1 0} facets rather than the most stable (1 1 1)-type facet [10,17]. Zhong *et al.* [18] reported that the exposed {1 0 1} and {0 2 0} faces of Co_2C nanoprisms had shown high selectivity for lower olefins as well as inhibit methane production in Fischer-Tropsch to olefins (FTO) field. Generally speaking, the different facets of metal nanoparticles result in quite different catalytic activities. Li's group [19] discovered that high index Co_3O_4(1 1 2) surface was more active than the basic {0 0 1} and {0 1 1} facets. Later they [20] demonstrated that the Co_3O_4 nanobelt exposed (0 1 1) surface was more active than Co_3O_4 nanocube exposed (0 0 1) surface for CO oxidation. Liu *et al.* [21] synthesized four Co_3O_4 crystals with different crystal planes and established the correlation between the crystal planes and the ability of water splitting as {1 1 1} > {1 1 2} > {1 1 0} > {0 0 1}. Gao *et al.* [22] disclosed that the exposed {1 1 2} surfaces of significant for CO_2 molecules activation and it could significantly enhance photocatalytic CO_2 reduction efficiency.

The recent studies had shown that metal nanoparticles would change their shape in the reactive environment with in situ observations [23–26]. Yoshida *et al.* [27] found that adsorbed CO molecules could cause the {1 0 0} surfaces of a gold nanoparticle to reshape during CO oxidation. In order to explore the changes of Co

* Corresponding authors.
E-mail addresses: wqiang@sxicc.ac.cn (Q. Wang), houbo@sxicc.ac.cn (B. Hou).

https://doi.org/10.1016/j.apsusc.2019.144469
Received 24 July 2019; Received in revised form 18 October 2019; Accepted 20 October 2019
Available online 29 October 2019
0169-4332/ © 2019 Elsevier B.V. All rights reserved.

nanoparticles, Kristin et al. [1] studied the surface of Co nanoparticle changes with the gas changing by using small-angle X-ray scattering (SAXS). Baldi *et al.* [28] used in situ electron energy-loss spectroscopy to detect the phase transitions of each palladium nanocrystals during hydrogen absorption and desorption. Hansen *et al.* [29] in situ transmission electron microscopy experiments observed that the copper nanocrystals change with changes in the gaseous environment. The multiscale structure reconstruction (MSR) modeling with in situ transmission electron microscopy (TEM) displayed the equilibrium shape of Au nanoparticles during under O_2 and H_2 atmospheres [6]. Thus, it is a vital step to predict whether and how the morphology of metal NPs changes in the reactive environment. Zhu and co-workers [30–32] had discovered that H_2O, CO, NO, O_2, or H_2 could effect on the equilibrium shape of metal NPs, which depend on temperature and pressure. Under N_2 pretreatment, Fe nanoparticles mainly exposed Fe(1 0 0) surface [33]. Fe(1 1 0) was the most exposed surface under the H_2 reduction environment [34]. The Mo single crystal showed only the (1 1 0), (2 1 1) and (1 0 0) surfaces were exposed in relatively high temperature and one hydrogen atmosphere, which was also in line with the X-ray diffraction (XRD) results [35]. Based on Wulff constructions, it could be found the structures of Pt could be adjusted by the adsorption of hydrogen [36]. These reactions usually involve interactions between mental NPs and the surrounding gas conditions (typically CO and hydrogen), which would change the morphology and surface structure.

Syngas (CO + H_2) on Co-based FTS catalysts could be converted into long-chain hydrocarbons [37–43]. Beitel *et al.* [44] firstly applied polarization modulation infrared reflection absorption spectroscopy to explore the restructuring of CO-induced Co(0001) surface restructuring under a high-pressure regime. Wilson [45] measured the restructuring of Co(0001) surface to triangular cobalt islands under CO hydrogenation conditions. Høydalsvik *et al.* [46] found that adsorbed CO molecules lead to atomic migration on Co surface. It had been confirmed that the CO-induced surface restructures with the aid of scanning tunneling microscopy (STM) [47]. Due to the complexity of the catalytic systems and the difficulty in situ observation the structural changes under real working conditions, there were limited studies from both experimental and theoretical aspects on the structural evolution of FCC cobalt nanoparticle under CO and hydrogen environments. For ideal equilibrium particle [48], Wulff construction of FCC Co particles predicts exposure of Co(1 0 0), Co(3 1 1), Co(1 1 0) and Co(1 1 1) surface terminations. Therefore, we employed spin-polarized DFT calculations and ab initio atomistic thermodynamics to investigate the equilibrium morphology evolution of four FCC Co surfaces under CO and hydrogen environment. In order to fill this gap, the atomic-scale observation of the shape evolution of Co nanoparticles under CO and hydrogen conditions at given temperature and reactive gas pressure would be investigated. In this work, two topics will be investigated by using DFT calculations with *ab initio* atomistic thermodynamics. (i) What is the effect on CO or hydrogen surface coverage by changing different temperature and partial pressure? (ii) How does the gas adsorption influence on the surface morphology of Co catalyst?

2. Computational details

2.1. Method and models

All the spin-polarized DFT calculations were carried out with Vienna Ab Initio Simulation Package (VASP) [49,50]. As a prevalent exchange-correlation potential, the Perdew-Burke-Ernzerh of functional within the generalized gradient approximation (GGA-PBE) was used [51]. The calculated equilibrium lattice constant for Co is 3.54 Å, in good consistent with previous theoretical [52] and experimental values [53]. In order to exclude interactions between the periodic slabs, neighboring slabs were divided by a 12 Å vacuum. The other parameters like the cutoff energy of plane wave and convergence criteria for the electronic self-consistent interactions were set 400 and 10^{-5} eV. Geometry optimizations were allowed to relax until the forces were smaller than 0.03 eV/Å. Besides, the *k*-point sampling was produced by a (3 × 3 × 1) mesh Monkhorst-Pack mesh [54]. Also, we used a three-layer *p*(3 × 3) model for FCC Co surfaces. When the geometries were optimized, the Co atoms in the top and the structure of the adsorbates were set to relax, and the bottom two layers of the slabs were fixed. Furthermore, the stepwise adsorption energy was employed to measure the most stable CO molecule configuration.

$$\Delta E_{ads} = E_{n+1CO/slab} - (E_{nCO/slab} + E_{CO}) \quad (1)$$

Besides, the adsorption energy (ΔE_{ads}) of H atoms could be defined as follows:

$$\Delta E_{ads} = E_{n+1H/slab} - (E_{nH/slab} + 1/2E_{H_2}) \quad (2)$$

The saturated adsorption with n molecules could be predicted by the positive ΔE_{ads} for n + 1 adsorption molecules.

2.2. Thermodynamics analysis

As an effective tool to address problems referring to environmental conditions, the *ab initio* atomistic thermodynamics had been widely used in many catalytic fields [55–61].

In the method part, the surface energy (γ) could be calculated based on Eq. (3)

$$\gamma(T, p) = \frac{1}{A}[G - \Sigma n_i \mu_i(T, p)] \quad (3)$$

where the Gibbs free energy of the solid surface is abbreviated as G; *A* represents the total surface area of the top and bottom equilibrium surfaces; $\mu_i(T, p)$ stands for the species chemical potential; n_i represents the i_{th} type species number, respectively.

Next, the surface energy with n_i gas adsorption could be defined as follows:

$$\gamma_{hkl}^{ads}(T, p, n_i) = \frac{1}{A}[G_{hkl}^{ads}(T, p, \{n_{gas}^{ads}\}) - \Sigma n_i \mu_i(T, p) \quad (4)$$

where$G_{hkl}^{ads}(T, p, \{n_{gas}^{ads}\})$ represents the Gibbs free energy absorbed n species on the (*hkl*) surface; $\mu_i(T, p)$ stands for all the species chemical potential in the system which the adsorbed species are included.

Then, the surface energy of Co surfaces with nCO molecules adsorbed could be defined as in Eq. (5) based on Eq. (4).

$$\gamma_{Co}^{ads}(T, p, nCO) = \frac{1}{A}[G_{Co}^{ads}(T, p, \{nCO\}) - n_{Co}\mu_{Co}(T, p) - n_{CO}\mu_{CO}(T, p)] \quad (5)$$

Furthermore, surface energy ($\gamma_{Co}^{clean}(T, p)$) of the clean Co surfaces could be given in Eq. (6)

$$\gamma_{Co}^{clean}(T, p) = \frac{1}{A}[G_{Co}^{clean}(T, p) - n_{Co}\mu_{Co}(T, p)] \quad (6)$$

where $G_{Co}^{clean}(T, p)$ is the Gibbs free energy of the clean Co surface; $\mu_{Co}(T, p)$ represents the bulk Go chemical potential. Combined with the formula (5) and (6), the surface free energy of the (*hkl*) surface absorbed with n CO molecules could be defined as Eq. (7)

$$\gamma_{Co}^{ads}(T, p, nCO) = \gamma_{Co}^{clean}(T, p) + \frac{1}{A}[G_{Co}^{ads}(T, p, \{nCO\}) - G_{Co}^{clean}(T, p) - n_{CO}\mu_{CO}(T, p)] \quad (7)$$

Following, in order to calculate the surface energy, the Gibbs free energy changes for CO adsorption process needs to be calculated. The derivation details of the method could be found in our previous work [62].

At different temperatures and pressures, the surface free energy of the surface absorbed with nCO molecules adsorption could be finally rewritten as Eq. (8).

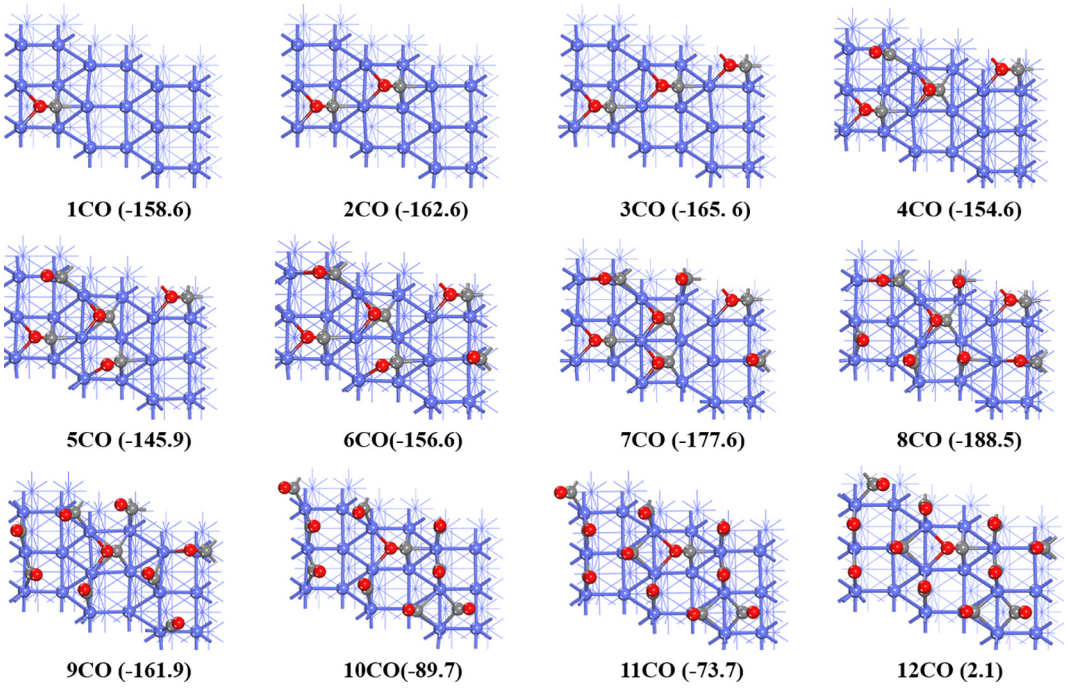

Fig. 1. Stepwise CO adsorption structures and energies (kJ/mol) on Co(3 1 1) surface. The Co, C and O atoms are plotted in purple, grey and red, respectively. (For interpretation of the references to colour in this figure legend, the reader is referred to the web version of this article.)

$$\gamma_{Co}^{ads}(T, p, \mathrm{nCO}) = \gamma_{Co}^{clean}(T, p) + \frac{1}{A}[\Delta G_{Co}^{ads}(T, p, \{\mathrm{nCO}\})] \quad (8)$$

The clean Co surface energy could be described as

$$\gamma_{Co}^{clean}(T, p) = \frac{1}{A}[E_{(\mathrm{Co(hkl)})} - \mathrm{n_{Co}}E_{\mathrm{Co-bulk}}] \quad (9)$$

where $E_{(Co(hkl))}$ represents the Co(hkl) surface's total energy of as well as $E_{\mathrm{Co-bulk}}$ is the bulk Co's total energy.

3. Results

3.1. CO adsorption at different coverage

In order to determine the most stable adsorption CO configurations at different coverage, the stepwise adsorption energies had been calculated by DFT calculations. Besides, the most stable adsorption structures, as well as the stepwise adsorption energies of CO molecules on Co(3 1 1), (1 1 1) and (1 1 0) are shown in Figs. 1–3.

The microcosmic adsorption and desorption of CO molecules at different coverage of Co(1 0 0) surface had been carried out and all CO molecules preferred the 4-fold hollow sites at the coverage of 1/9–3/9 ML in our previous work [62]. Furthermore, CO molecules were more likely located at the bridge site with the increase of CO coverage, and the corresponding adsorption energies gradually decrease. It was found that 7/9 ML was the saturated coverage on Co(1 0 0) surface.

As displayed in Fig. 1, the adsorption energy of CO molecule located at the B5 step site on the Co(3 1 1) surface is −158.6 kJ/mol which is in accordance with the previous report [48]. At the coverage from 2CO to 3CO, all the CO are still adsorbed at B5 step sites, it could be found that the difference of adsorption energies among them are quite small, indicating very weak repulsive interactions among these CO molecules. With CO coverage increasing, the adsorption states are no longer regular. For example, at n_{CO} = 11, it is possible to form the coexistence of B5, bridge, hcp, fcc and 4-fold hollow site adsorption geometries. The saturated coverage is reached at n_{CO} = 11 because of the positive value (2.1 kJ/mol) at n_{CO} = 12. However, these transformations do not lead

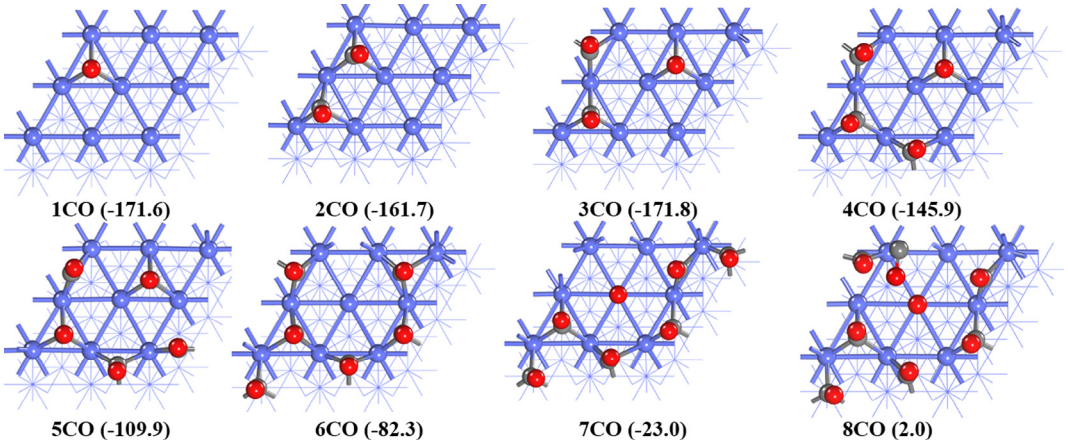

Fig. 2. Stepwise CO adsorption structures and energies (kJ/mol) on Co(1 1 1) surface. The Co, C and O atoms are plotted in purple, grey and red, respectively. (For interpretation of the references to colour in this figure legend, the reader is referred to the web version of this article.)

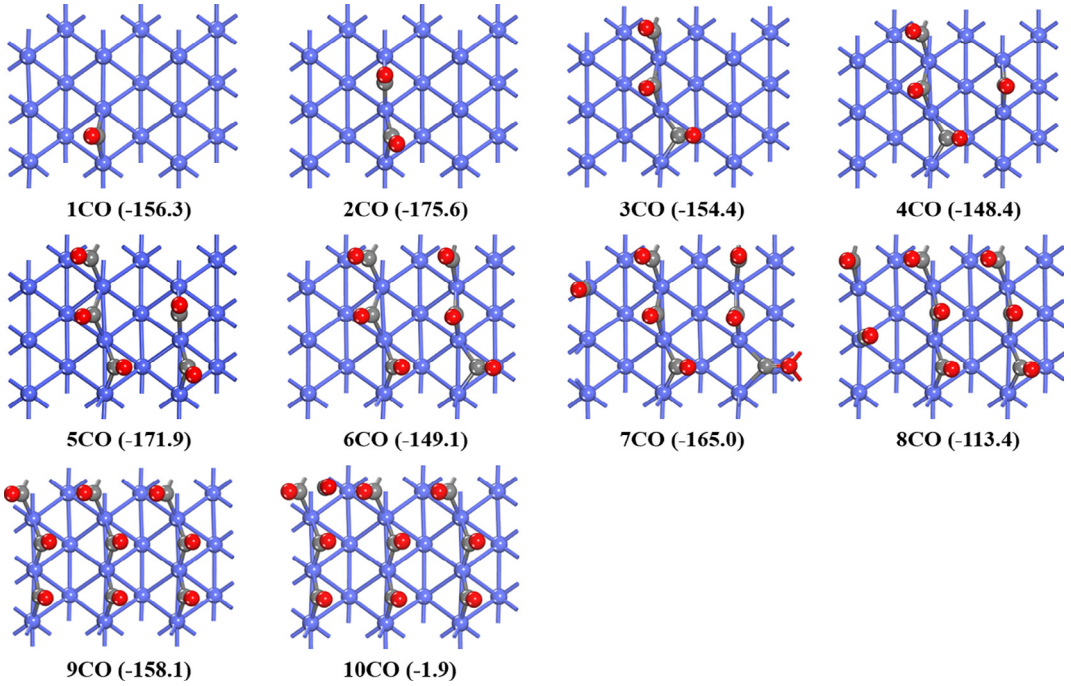

Fig. 3. Stepwise CO adsorption structures and energies (kJ/mol) on Co(1 1 0) surface. The Co, C and O atoms are plotted in purple, grey and red, respectively. (For interpretation of the references to colour in this figure legend, the reader is referred to the web version of this article.)

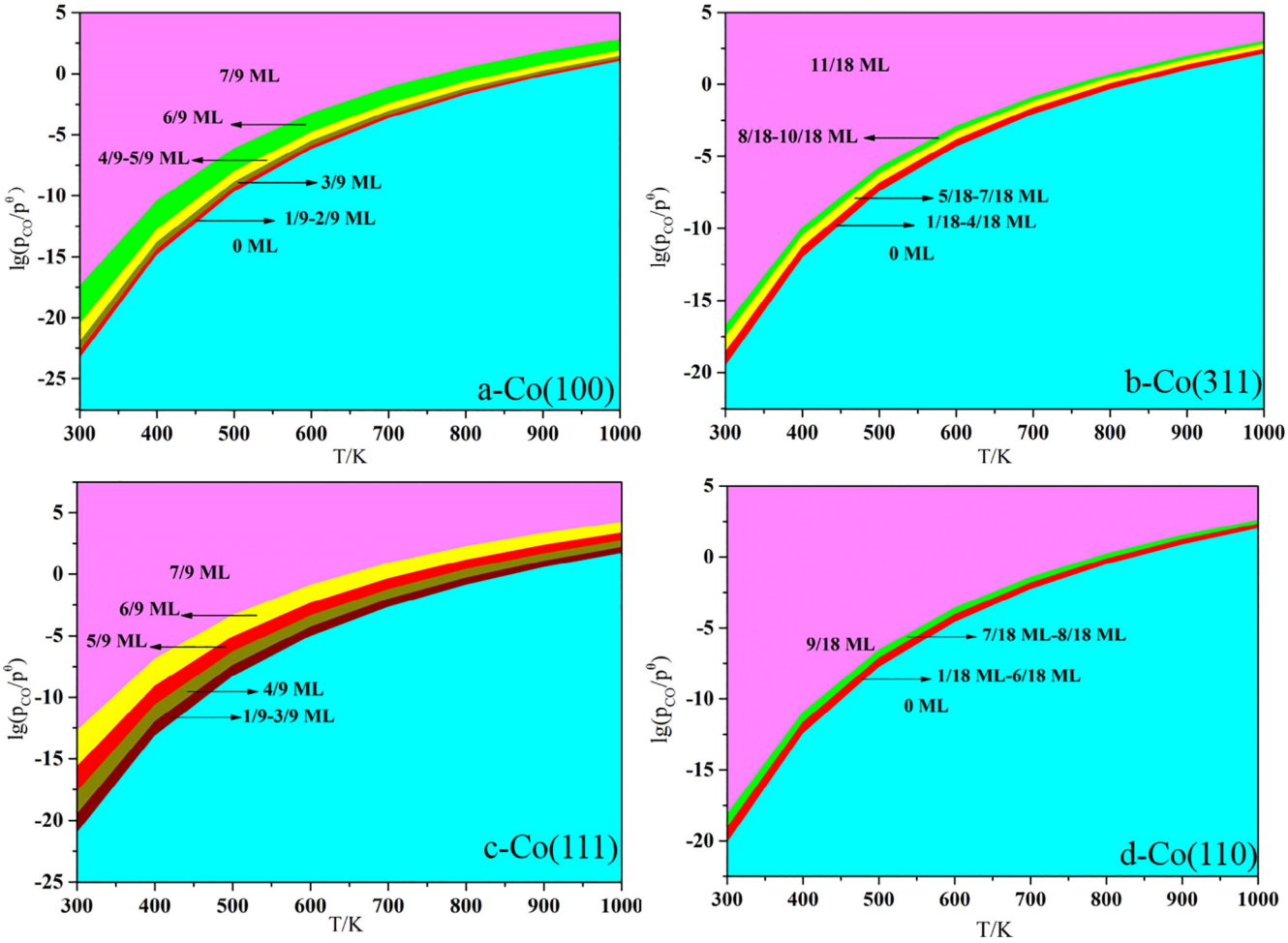

Fig. 4. Phase diagrams of stable CO coverage on Co(1 0 0) surface (a), Co(3 1 1) (b), Co(1 1 1) (c) and Co(1 1 0) (d) under different conditions.

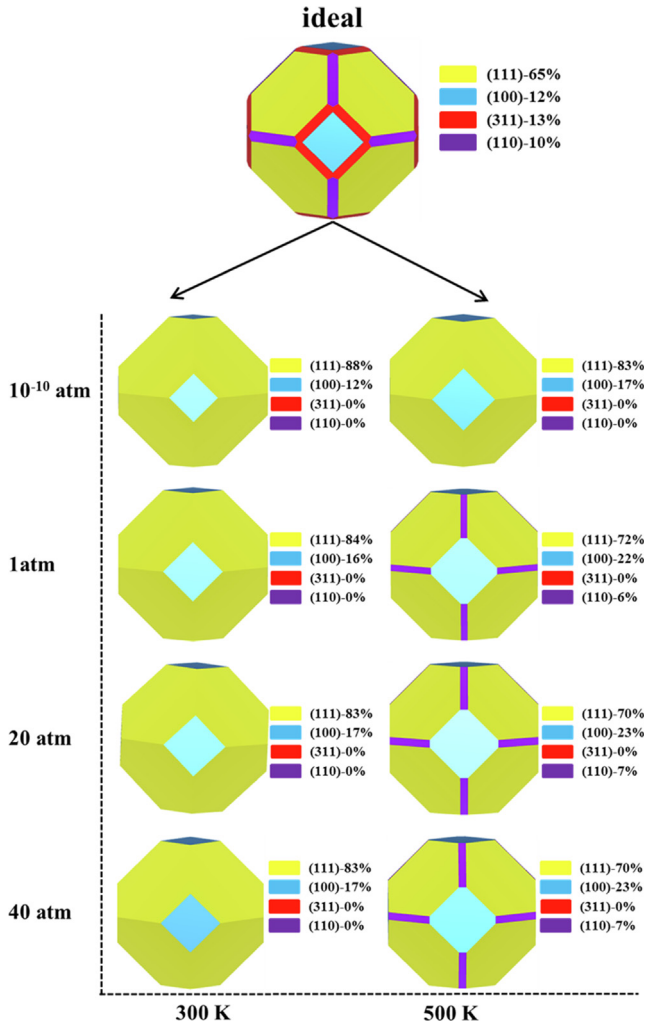

Fig. 5. Morphologies of the metal FCC Co catalyst under different CO atmosphere.

to the reconstruction of Co(3 1 1) surface.

As depicted in Fig. 2, CO molecule on the Co(1 1 1) surface prefers the hcp site with the energy of −171.6 kJ/mol, which is in line with the previous studies on Co(1 1 1) [48,63]. Saeys *et al.* [64] found that the adsorption energy of CO on a clean Co(1 1 1) surface was 130.0 kJ/mol under F-T conditions (500 K, 20 bar, 60% conversion), which was lower than our calculated. The difference could be explained by the influence of temperature and pressure on the adsorption energy. Generally, the stepwise energies would gradually decrease with the increase of the CO molecules coverage. When the number of CO molecules ranges from 1 to 3, the CO molecules have similar stepwise adsorption energies, although the third CO molecule would like to adsorb at the fcc site. At n_{CO} = 5, the stepwise energy decreases to −109.9 kJ/mol, it appears the bridge configuration. Three kinds of adsorption configurations (top, fcc, hcp) would coexist on the surface at n_{CO} = 7, but the bridge adsorption configuration amazingly disappears. Furthermore, the saturated coverage is 7/9 ML, because of the positive adsorption energy (2.0 kJ/mol) at n_{CO} = 8 on Co(1 1 1) surface. Similarly, there is also no reconstruction of Co(1 1 1) upon CO molecule adsorption.

As indicated in Fig. 3, the adsorption energy of one CO molecule adsorbed at the bridge site is −156.3 kJ/mol, which is in agreement with the previous study on Co(1 1 0) [48]. The saturation coverage has 9 CO molecules and all form the most stable adsorption at the bridge sites. However, at n_{CO} = 7, the top site becomes favorable and part of the bridge site reconstructs into the top site. theoretical, the bond length of C-O of CO molecule is longer from 1.18 to 1.24 Å. It could be concluded that lateral repulsions became significant. When n_{CO} > 7, the top adsorption configuration disappears. More importantly, surface reconstruction is not obvious during CO adsorption, due to the regular arrangement of CO molecules at different coverage.

As discussed above, the saturated coverage of CO molecule on the Co(1 0 0), (3 1 1), (1 1 1), and (1 1 0) surfaces are 7/9, 11/18, 7/9, and 9/18 ML, respectively. The molecular adsorption configuration is affected by the lateral repulsive interaction becomes stronger with the increase of CO coverage.

Previous studied results had demonstrated that the projected density of states (PDOS) could analysis the binding energies of H_2 or CO molecules on different sites on various surfaces [65,66]. Therefore, to further understand the interaction between CO molecule and Co surfaces, the PDOS of one molecule CO adsorption on different sites on Co (3 1 1) surface was calculated, as shown in Fig. S1. From Fig. S1, one can clearly see that the total DOS of the adsorbed CO molecule shifts to lower energies compared to the total of a free CO molecule for the Co (3 1 1) surface. In addition, from Fig. S1(b) to Fig. S1(e), the total DOS of CO molecule adsorption on B5 active site shifts to much deeper lower energies than of that on the other sites. As discussed above, CO molecule on the Co(3 1 1) surface prefers the B5 site. The results explain that DOS with deeper lower energy means the most stable adsorption state. The corresponding PDOS of CO molecule adsorption on Co(1 1 1), Co (1 1 0) and Co(1 0 0) surfaces are depicted in Fig. S2, Fig. S3 and Fig. S4. Obviously, the trends for the stability of CO adsorption on Co(1 1 1), Co (1 1 0) and Co(1 0 0) are nearly the same as the result for Co(3 1 1), so we don't describe them again here.

3.2. Hydrogen adsorption at different coverage

In our previous work, we proved that H_2 would exist as the dissociative H atoms form from low to high coverage on the Co surfaces under real working conditions [67,68]. Thus, hydrogen atom adsorption is used as our research object. To explore the most stable configuration at different coverage, all possible hydrogen atoms adsorption configurations at individual coverage on FCC Co surfaces were calculated. H atoms on Co(1 0 0), (3 1 1), (1 1 1) and (1 1 0) wherein the most stable adsorption structures are depicted in Supplementary Material Fig. S5–8.

On the Co(1 0 0) surface, the adsorption energy of the most stable hydrogen atom adsorption forms at the 4-fold hollow site is −42.7 kJ/mol. The most suitable adsorption site and adsorption energy of Co (1 0 0) presented here are the same as that proposed by Weststrate *et al.* [69] on the Co(1 0 0). Meanwhile, they presented that the most stable adsorption structure remains the hollow site when the hydrogen coverage increases to θ = 1 ML. The results of hydrogen adsorption configurations and energies from low to high coverage are presented in Supplementary Material Fig. S5. The saturation coverage has 9 hydrogen atoms (1 ML) and all perfer the 4-fold hollow sites. It is noted there are small difference of hydrogen adsorption energies at different coverage. Over the whole coverage, the stepwise adsorption energies are all approximately −45.0 kJ/mol.

On the Co(3 1 1) surface, it could be found that the adsorption energy of the most stable of H atom which adsorbed at the fcc site is −44.2 kJ/mol. At n_H < 9, all hydrogen atoms prefer the fcc sites with the close stepwise adsorption energies of −43.0 kJ/mol. At n_H = 9, for one of the hydrogen atoms, the most stable adsorption structure could alter from fcc site to bridge site despite the small changes of adsorption energy. At n_H > 9, three adsorption configurations (fcc, bridge, 4-fold hollow) would coexist on the surface, the stepwise adsorption energies of hydrogen atoms are approximate −30.0 kJ/mol. At the saturated coverage (n_H = 18), fcc and 4-fold hollow adsorption structures coexist on the surface, and the bridge adsorption configuration disappears. Moreover, all hydrogen atoms are regularly absorbed on the surface.

On the Co(1 1 1) surface, H atom prefers to anchor at the fcc site,

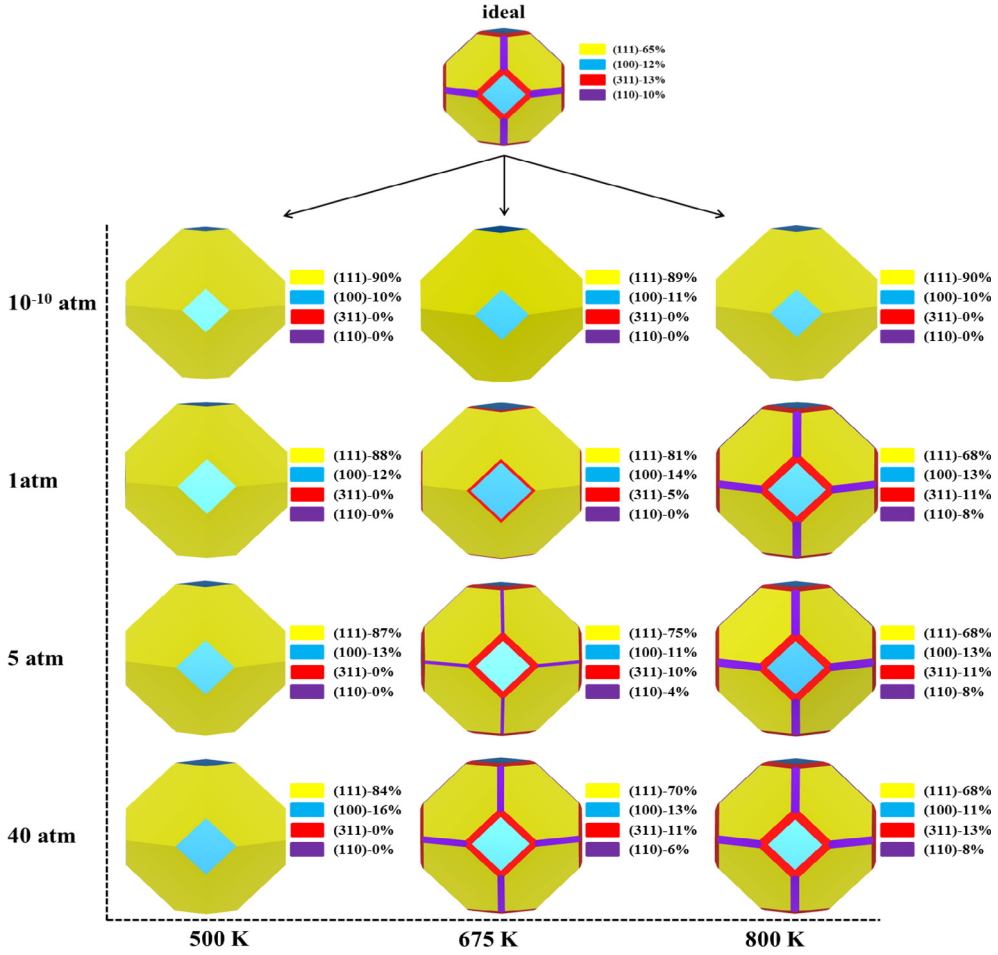

Fig. 6. Morphologies of the metal FCC Co catalyst under different hydrogen atmosphere.

which is consistent with the results reported previously [70]. Interestingly, the hcp adsorption configuration would gradually appear with the increase of H coverage. For example, at n_H = 4, 6, 7, the part of hydrogen atoms wherein the most stable adsorption configuration would switch from fcc sites to hcp sites. However, all hydrogen atoms are regularly absorbed at the fcc site when the coverage is increased to 1 ML. Moreover, the stepwise adsorption energy is up to −73.7 kJ/mol, which is greater than that of other coverage.

The most stable adsorption position of one hydrogen atom on the (1 1 0) surface is located at the 3-fold hollow site and the adsorption energy is −36.4 kJ/mol. The first six H atoms (n_H = 1–6) present similar stepwise adsorption energies (−35.0 kJ/mol), and all prefer the 3-fold hollow site. At n_H = 7–9, H atoms start to anchor at the bridge site. The stepwise adsorption energies generally decrease, with increasing H coverage. When n_H = 14, it is the saturated coverage because of the positive value (0.1 kJ/mol) for n_H = 15. Besides, 3-fold hollow and bridge site adsorption configurations would coexist on the surface.

According to above results, the saturated coverage of H atom on the Co(1 0 0), (3 1 1) and (1 1 1) surfaces are 1 ML, whereas on Co(1 1 0) surface is 7/9 ML. Their diverse hydrogenation abilities could be reflected by the small difference in the H atom numbers adsorbed on these surfaces. This suggests that it is insensitive for hydrogen adsorption on FCC Co.

3.3. Stable CO and hydrogen coverage under different conditions

The stability of the surface species coverage is always linked to temperature and pressure in practical experiments. To get meaningful information about the influence of pressure and temperature on the adsorption as well as desorption states, the Co surfaces under different conditions at individual coverage have been discussed. The phase diagram in Fig. 4 displays the relationship between the CO stable coverage and pressure and temperatures over four cobalt surfaces. There are several stable adsorption regions in each phase diagram, and it provides the possibility to stabilize CO coverage in each region as changing temperature and partial pressure of CO. For example, on the Co(3 1 1) surface, there are mainly six regions. Due to their similar adsorption energy and weak repulsive interaction, there is the coverage of 1/18 ML to 4/18 ML, 5/18 ML to 7/18 ML overlapped in the same region. From the phase diagrams, some meaningful information about the stable CO coverage depending on temperature and pressure is obtained as follows. At given temperature, as the CO partial pressure increases, the stable CO coverage increases. However, the coverage of CO on the surface reduces when the temperature is increased at given CO partial pressure. In addition, it is easy to obtain the temperatures for full CO desorption. For example, at $p_{CO} = 10^{-5}$ atm, the temperatures for full CO desorption on the (1 0 0), (3 1 1), (1 1 1), and (1 1 0) surfaces are about 650, 560, 620, and 600 K, respectively. Furthermore, under the same condition, we could also directly get the differences among the four Co surfaces in stable CO coverage. At T = 500 K and $p_{CO} = 10^{-5}$ atm condition, the most stable CO coverage is 7/9 ML on Co(1 0 0), 11/18 ML on Co(3 1 1), 6/9 ML on Co(1 1 1) and 1/2 ML on Co(1 1 0) surface, respectively. The phase diagrams about the relationship between the H stable coverage and pressure/temperature over four cobalt surfaces are shown in Fig. S9. Obviously, the trend for the stable hydrogen coverage is nearly the same as the results about the stable CO coverage under different conditions.

3.4. Morphology of FCC Co under CO and hydrogen atmosphere

Knowledge of the equilibrium morphology evolution and structure of the exposed surface of FCC cobalt nanoparticles is significant for understanding and tuning their catalytic performance. According to the surface energies, the equilibrium morphological shape of the cobalt nanoparticles is evaluated using the Wulff construction. The surface energies (E_s) and exposed ratios (S_s) of each surface under ideal condition are listed in Table S1. It clearly shows that the Co(1 1 1) facet cover predominantly 65% of the total distribution with relatively lowest surface energy. The values of the surface energies of four Co surfaces Co(3 1 1), Co(1 0 0), Co(1 1 0), and Co(1 1 1) are 161, 159, 157 and 134 meV/Å^2, respectively. This result is in accordance with is in line with the previous work [48]. In addition, the estimated surface proportions increased by the order of Co(1 1 0) < Co(1 0 0) < Co (3 1 1) < Co(1 1 1). It has been reported [71] that the surface free energies of (1 0 0), (1 1 1) and (1 1 0) surfaces are in accordance to $E_s(1\,0\,0) > E_s(1\,1\,0) > E_s(1\,1\,1)$ for FCC-Co structure.

FTS is an alternative route to produce various value-added chemicals via syngas (CO + H_2), and CO adsorption and activation are the vital steps in FTS mechanism.[15,52,64,72,73] Therefore, it is of great significance to investigate the surface morphology modified by CO adsorption. According to the CO adsorption energies at different coverage, the surface energies of each facet at different temperatures and CO partial pressures had been calculated and listed in Table S2–3. It could be found that the surface energies would be reduced by the CO adsorption and also impacted the stabilities of surface. In addition, the CO partial pressure increases, accompanied by the increase of surface energies, which may cause by stronger CO-CO repulsions leading to the weaker of CO-Co metal interaction. According to the surface energies of each facet, Wulff construction is applied in characterizing the morphologies of the Co catalyst at different temperatures and pressures, which is given in Fig. 5. According to Wulff's rule, the contribution of crystals to exposed surface areas is attributed to surface free energy and orientation. CO adsorption could significantly affect the ratio of morphology to the exposed surface. For instance, at $T = 300$ K, with the increase of CO partial pressure, the ratio of the Co(1 0 0) surface increases while Co(1 1 1) surface decreases, Co(3 1 1) and (1 1 0) disappear, but the most exposed surface always is Co(1 1 1). Considering for instance the FTS typically operating at ~500 K, with the increase of CO partial pressure from 10^{-10} to 20 atm, the ratio of the (1 1 1) surface decreases from 83% to 70% while Co(1 0 0) increases from 17% to 23%; The cobalt nanoparticles are not exposed to Co(1 1 0) surface at low temperature, but Co(1 1 0) surface appear at high temperature. It suggests that the Co(1 1 1) surface is most exposed among all surfaces under various conditions. The calculated CO activation energy showed that the Co(1 1 0) surface exhibits higher activity in CO direct dissociation than that of Co(1 1 1) surface [48]. Although the Co(1 1 0) surface covers 7% of the surface area, exposure of eight equivalent Co (1 1 0) facets possessing relatively highly active sites is located to the edges of the Wulff shape.

Generally speaking, cobalt-based FTS catalysts consists of cobalt in its metallic form (Co^0), which was reduced under a hydrogen atmosphere prior to the experiment [74–77]. Therefore, the description of the morphology of cobalt nanoparticle changed induced by hydrogen adsorption would be critical for tuning its catalytic activities. As shown in Tables S4–6, it clearly revealed that hydrogen adsorption on cobalt surfaces resulted in surface energies decrease. It is remarkable that the change of the surface energies of four cobalt facets by adsorption hydrogen is less than that CO adsorption. It can be explained that CO has much larger binding energies than hydrogen. To study the changes in Co morphology with temperature, three different temperatures (500, 675, and 800 K) at $p_{H_2} = 5$ atm had been chosen and shown in Fig. 6. At $T = 500$ K, the most exposed surface is Co(1 1 1) with a high ratio of 87%, and the exposed ratio of Co(1 0 0) from 12% increase to 13% compared to ideal condition. However, Co(3 1 1) and (1 1 0) facets disappear under this condition with high surface energies. When the temperature increases to 675 K, Co(3 1 1) and (1 1 0) facets with relatively lower surface energies represent close to 14% of the total distribution the Co Wulff shape, and the proportion of Co(1 1 1) surface reduced from 87% to 75%. As the temperature keeps rising, the surface area ratios of Co catalyst present a slight variation. Since most catalysts were activated with flowing H_2 at 400–450 °C, 0.10 MPa [76,77], we here chose $T = 675$ K to discuss the changes of cobalt morphology with increasing pressure. At $p_{H_2} = 10^{-10}$ atm, Co(1 1 1) facet with relatively lowest surface energies represents close to 89% of the total distribution, and Co(1 0 0) facet represents 11% of the surface. Under this condition, Co(3 1 1) and (1 1 0) facets disappear compared with the idea equilibrium shape of FCC Co. When the pressure increases to 5 atm, the Co (1 1 1) surface, which exhibits the lowest surface energy, has a predicted surface fraction of 75%, and the remaining 25% is made up by Co(1 0 0), (3 1 1), (1 1 0) facets. When the Co_3O_4 catalysts were reduced in flowing H_2, the reduced sample consisted primarily of FCC Co(1 1 1) and some unreduced CoO [78]. With the increase of pressure, the proportion of Co(3 1 1) and (1 1 0) facets present a little increase, and the Co(1 1 1) surface is still the most abundant. The facets exposed the B5 sites have been proposed to be the active site for CO dissociation [52,64,79]. Meanwhile, step Co(3 1 1) and Co(1 1 0) facet remain able to form very favorable B5-type sites [80]. This work well reveals that temperature and pressure can influence the facets distribution and the exposure of the active sites, favoring the CO activation.

Through the overall influence of CO and hydrogen environments on equilibrium morphology evolution of FCC cobalt nanoparticle described above, it had shown that the most exposed surface was Co(1 1 1) within a large range of temperatures and pressures under hydrogen and CO atmosphere, and step surface Co(3 1 1) is the least stable surface of FCC Co structure. However, it has been reported [48,62,63] that CO dissociation on Co(1 1 1) has the highest active energy compared to Co (3 1 1), (1 1 0) and (1 0 0) surfaces. In other words, it is suggested to increase the ratio of Co(3 1 1) surface in the cobalt-based catalyst of FTS to improve the reactive activity. That is to say, reduction and reaction conditions can change the morphologies of cobalt nanoparticles, then causing the difference of their catalytic. Taking the maneuverability of experiment and catalytic performance into account, it is reasonable to select 675 K and 5 atm as H_2 reduction condition. This assists in designing better active and selective new catalytic materials by giving priority to more active surfaces or by increasing the activity density. Therefore, how to increase the area of step or kink surfaces, such as Co (3 1 1) surface, is meaningful and challenging work. This purpose could also realize by doping metal or metallic oxide promotion. It is worth noting that it can affect the corresponding morphology of metallic Co and subsequent reactivity when Mn promoter is added. Zheng *et al.* [81] confirmed that the exposed Co(1 0 0) increases to a large extent with Mn promoter instead of the exposed Co(0 0 2) during the reduction-carburization-reduction treatment. Huo *et al.* [82] revealed that potassium promoter can modify the crystallographic orientation of Fe, as well as more active facets such as Fe(2 1 1) and Fe(3 1 0) become the energetically favored. Therefore, in our future work, we expect to describe the equilibrium structures of cobalt nanoparticles interacting with a mixed reaction gas and tune the morphology of cobalt nanoparticles with abundant highly active facets by doping metal promoter.

4. Conclusions

Combining spin-polarized density functional theory and *ab initio* atomistic thermodynamics, CO, as well as hydrogen adsorption on the Co(1 0 0), (3 1 1), (1 1 1) and (1 1 0) surfaces had been investigated to predict the equilibrium morphology evolution of FCC cobalt nanoparticle under CO and hydrogen environments.

According to our calculation results, the saturated coverage of CO molecule on the Co(1 0 0), (3 1 1), (1 1 1), (1 1 0) surfaces is 7/9, 11/18, 7/9 and 1/2 ML, respectively. For hydrogen adsorption, there is the

lowest saturated coverage (7/9 ML) on Co(1 1 0) surface, followed by the other surface (1 ML). Besides, surface reconstruction upon CO or hydrogen adsorption is not obvious among these surfaces. From the phase diagrams, it could provide important information about temperature-programmed desorption data detected by experiment at ultrahigh vacuum conditions or any given pressure. For example, the predicted temperature of CO desorption on Co(1 0 0) at 650 K, on Co (3 1 1) at 560 K, on Co(1 1 1) at 620 K, and on Co(1 1 0) at 600 K, at $p_{CO} = 10^{-5}$ atm.

Based on surface energies of four surfaces, Wulff construction is applied in characterizing the role of the CO or hydrogen adsorption on the Co morphology at different (T, p) condition. With the increasing temperature at given hydrogen or CO partial pressure, the exposed ratio of the Co(1 1 0) surface increases while that of (1 1 1) surface decreases. At the typical temperature (675 K) of hydrogen reduction, the estimated surface proportion of the Co(3 1 1) exposed the B5 site exist a marked increase, which consistent with commonly experiment hydrogen reduction temperature for Co catalyst. This clearly indicates the structure and morphology of the catalyst depends on the environment. This work can not only promote to describe the relationship between surface morphology and activity site of catalysts but also give insights into the shape evolutions of Co nanoparticle under CO and hydrogen environments.

Declaration of Competing Interest

There are no conflicts of interest to declare.

Acknowledgments

The work was supported by the National Natural Science Foundation of China (No. 21736007, 21872162 and U1710104), and the "Transformational Technologies for Clean Energy and Demonstration", Strategic Priority Research Program of the Chinese Academy of Sciences (No. XDA 21020202) and the ShanXi Provincial Research Foundation for Basic Research (No. 201701D221242). The authors are grateful to Lvliang's cloud computing center for computational resources by the Tianhe-2.

Appendix A. Supplementary material

Supplementary data to this article can be found online at https://doi.org/10.1016/j.apsusc.2019.144469.

References

[1] K.B. Zhou, Y.D. Li, Angew. Chem. Int. Ed. 51 (2012) 602–613.
[2] M. Zhao, A.O. Elnabawy, M. Vara, L. Xu, Z.D. Hood, X. Yang, K.D. Gilroy, L.F. Cosme, M. Chi, M. Mavrikakis, Y. Xia, Chem. Mater. 29 (2017) 9227–9237.
[3] H.H. Ye, Q.X. Wang, M. Catalano, N. Lu, J. Vermeylen, M.J. Kim, Y.Z. Liu, Y.G. Sun, X.H. Xia, Nano Lett. 16 (2016) 2812–2817.
[4] S. Qing, Z.J. Zhang, J. Am. Chem. Soc. 126 (2004) 6164–6168.
[5] J. Watt, C. Yu, S.L.Y. Chang, S. Cheong, R.D. Tilley, J. Am. Chem. Soc. 135 (2013) 606–609.
[6] A. Chmielewski, J. Meng, B. Zhu, Y. Gao, H. Guesmi, H. Prunier, D. Alloyeau, G. Wang, C. Louis, L. Delannoy, P. Afanasiev, C. Ricolleau, J. Nelayah, ACS Nano 13 (2019) 2024–2033.
[7] X. Yu, Y. Shan, K. Chen, Appl. Surf. Sci. 439 (2018) 298–304.
[8] K. Lee, M. Kim, H. Kim, J. Mater. Chem. 20 (2010) 3791.
[9] W.W. Wang, W.Z. Yu, P.P. Du, H. Xu, Z. Jin, R. Si, C. Ma, S. Shi, C.J. Jia, C.H. Yan, ACS Catal. 7 (2017) 1313–1329.
[10] K.B. Zhou, X. Wang, X.M. Sun, Q. Peng, Y.D. Li, J. Catal. 229 (2005) 206–212.
[11] J. Pal, T. Pal, Nanoscale 7 (2015) 14159–14190.
[12] Y. Li, Q.Y. Liu, W.J. Shen, Dalton Trans. 40 (2011) 5811–5826.
[13] P. Lara, O. Rivada Wheelaghan, S. Conejero, R. Poteau, K. Philippot, B. Chaudret, Angew. Chem. Int. Ed. 50 (2011) 12080–12084.
[14] J.A. van Bokhoven, ChemCatChem 1 (2009) 363–364.
[15] W.Z. Li, J.X. Liu, J. Gu, W. Zhou, S.Y. Yao, R. Si, Y. Guo, H.Y. Su, C.H. Yan, W.X. Li, Y.W. Zhang, D. Ma, J. Am. Chem. Soc. 139 (2017) 2267–2276.
[16] N.D. Spencer, R.C. Schoonmaker, G.A. Somorjai, J. Catal. 74 (1982) 129–135.
[17] M. Huang, S. Fabris, J. Phys. Chem. C 112 (2008) 8643–8648.
[18] L.S. Zhong, F. Yu, Y.L. An, Y.H. Zhao, Y.H. Sun, Z.J. Li, T.J. Lin, Y.J. Lin, X.Z. Qi, Y.Y. Dai, L. Gu, J.S. Hu, S.F. Jin, Q. Shen, H. Wang, Nature 538 (2016) 84–87.
[19] L.H. Hu, Q. Peng, Y.D. Li, J. Am. Chem. Soc. 130 (2008) 16136–16137.
[20] L.H. Hu, K.Q. Sun, Q. Peng, B.Q. Xu, Y.D. Li, Nano Res. 3 (2010) 363–368.
[21] L. Liu, Z.Q. Jiang, L. Fang, H.T. Xu, H.J. Zhang, X. Gu, Y. Wang, ACS Appl. Mater. Inter. 9 (2017) 27736–27744.
[22] C. Gao, Q.Q. Meng, K. Zhao, H.J. Yin, D.W. Wang, J. Guo, S.L. Zhao, L. Chang, M. He, Q.X. Li, H.J. Zhao, X.J. Huang, Y. Gao, Z.Y. Tang, Adv. Mater. 28 (2016) 6485–6490.
[23] B. Eren, D. Zherebetskyy, L.L. Patera, C.H. Wu, H. Bluhm, C. Africh, L.W. Wang, G.A. Somorjai, M. Salmeron, Scenice 351 (2016) 475–478.
[24] X. Zhang, J. Meng, B.E. Zhu, J. Yu, S.H. Zou, Z. Zhang, Y. Gao, Y. Wang, Chem. Commun. 53 (2017) 13213–13216.
[25] T. Avanesian, S. Dai, M.J. Kale, G.W. Graham, X.Q. Pan, P. Christopher, J. Am. Chem. Soc. 139 (2017) 4551–4558.
[26] H. Zhang, M.S. Jin, Y.J. Xiong, B. Lim, Y.N. Xia, Acc. Chem. Res. 46 (2013) 1783.
[27] H. Yoshida, Y. Kuwauchi, J.R. Jinschek, K.J. Sun, S. Tanaka, M. Kohyama, S. Shimada, M. Haruta, S. Takeda, Scenice 335 (2012) 317–319.
[28] A. Baldi, T.C. Narayan, A.L. Koh, J.A. Dionne, Nature Mater. 13 (2014) 1143–1148.
[29] P.L. Hansen, J.B. Wagner, S. Helveg, J.R. Rostrup Nielsen, B.S. Clausen, H. Tops¿e, Scenice, 295 (2002) 2053–2055.
[30] B.E. Zhu, J. Meng, Y. Gao, J. Phys. Chem. C 121 (2017) 5629–5634.
[31] J. Meng, B.E. Zhu, Y. Gao, J. Phys. Chem. C 122 (2018) 6144–6150.
[32] B.E. Zhu, Z. Xu, C.L. Wang, Y. Gao, Nano Lett. 16 (2016) 2628–2632.
[33] T. Wang, X.X. Tian, Y. Yang, Y.W. Li, J.G. Wang, M. Beller, H.J. Jiao, J. Phys. Chem. C 120 (2016) 2846–2854.
[34] T. Wang, S. Wang, Q. Luo, Y.W. Li, J.G. Wang, M. Beller, H.J. Jiao, J. Phys. Chem. C 118 (2014) 4181–4188.
[35] T. Wang, X.X. Tian, Y. Yang, Y.W. Li, J.G. Wang, M. Beller, H.J. Jiao, Phys. Chem. Chem. Phys. 18 (2016) 6005–6012.
[36] Q. Shi, R. Sun, Comput. Theor. Chem. 1106 (2017) 43–49.
[37] J.P. den Breejen, P.B. Radstake, G.L. Bezemer, J.H. Bitter, V. Frøseth, A. Holmen, K.P. de Jong, J. Am. Chem. Soc. 131 (2009) 7197–7203.
[38] Y.F. Yang, L.T. Jia, B. Hou, D.B. Li, J.G. Wang, Y.H. Sun, J. Phys. Chem. C 118 (2013) 268–277.
[39] Y.F. Yang, L.T. Jia, B. Hou, D.B. Li, J.G. Wang, Y.H. Sun, ChemCatChem 6 (2014) 319–327.
[40] G.L. Bezemer, J.H. Bitter, H.P.C.E. Kuipers, H. Oosterbeek, J.E. Holewijn, X.D. Xu, F. Kapteijn, A. Jos van Dillen, K.P. de Jong, J. Am. Chem. Soc. 128 (2006) 3956–3964.
[41] Y. Yang, L.T. Jia, B. Hou, D.B. Li, J.G. Wang, Y.H. Sun, Catal. Sci. Technol. 4 (2014) 717–728.
[42] B.A.F. Kengne, A.M. Alayat, G. Luo, A.G. McDonald, J. Brown, H. Smotherman, D.N. McIlroy, Appl. Surf. Sci. 359 (2015) 508–514.
[43] M.J. Parnian, A. Taheri Najafabadi, Y. Mortazavi, A.A. Khodadadi, I. Nazzari, Appl. Surf. Sci. 313 (2014) 183–195.
[44] G.A. Beitel, A. Laskov, H. Oosterbeek, E.W. Kuipers, J. Phys. Chem. 100 (1996) 12494–12502.
[45] J. Wilson, C.D. Groot, J. Phys. Chem 99 (1995) 7860–7866.
[46] K. Høydalsvik, J.B. Fløystad, A. Voronov, G.J.B. Voss, M. Esmaeili, J. Kehres, H. Granlund, U. Vainio, J.W. Andreasen, M. Rønning, D.W. Breiby, J. Phys. Chem. C 118 (2014) 2399–2407.
[47] H.J. Venvik, A. Borg, C. Berg, Surf. Sci. 397 (1998) 322–332.
[48] J.X. Liu, H.Y. Su, D.P. Sun, B.Y. Zhang, W.X. Li, J. Am. Chem. Soc. 135 (2013) 16284–16287.
[49] G. Kresse av, J. Furthmiiller, Comp. Mate. Sci. 6 (1996) 15–50.
[50] G. Kresse, J. Furthmüller, Phys. Rev. B 54 (1996) 11169–11186.
[51] J.P. Perdew, K. Burke, M. Ernzerhof, Phys. Rev. Lett. 77 (1996) 3865–3868.
[52] M.A. Petersen, J.A. van den Berg, I.M. Ciobîcă, P. van Helden, ACS Catal. 7 (2017) 1984–1992.
[53] P.H., D. Menzel, Surf. Sci. 93 (1980) 431–452.
[54] H.J. Monkhorst, J.D. Pack, Phys. Rev. B 13 (1976) 5188–5192.
[55] K. Reuter, M. Scheffler, Phys. Rev. B 68 (2003) 045407.
[56] K. Reuter, M. Scheffler, Phys. Rev. B 65 (2001) 035406.
[57] Z.J. Zuo, N. Li, S.Z. Liu, P.-D. Han, W. Huang, Appl. Surf. Sci. 366 (2016) 85–94.
[58] S.P. Sun, J.L. Zhu, S. Gu, X.P. Li, W.N. Lei, Y. Jiang, D.Q. Yi, G.H. Chen, Appl. Surf. Sci. 467–468 (2019) 753–759.
[59] X.H. Yu, X.M. Zhang, S.G. Wang, G. Feng, Appl. Surf. Sci. 343 (2015) 33–40.
[60] W.X. Li, C. Stampfl, M. Scheffler, Phys. Rev. B 68 (2003) 165412.
[61] F. Zasada, W. Piskorz, S. Cristol, J.F.O. Paul, A. Kotarba, Z. Sojka, J. Phys. Chem. C 114 (2010) 22245–22253.
[62] C.B. Chen, Q. Wang, R.G. Zhang, B. Hou, D.B. Li, L.T. Jia, B.J. Wang, Appl. Catal., A 523 (2016) 209–220.
[63] C.B. Chen, Q. Wang, G.R. Wang, B. Hou, L.T. Jia, D.B. Li, J. Phys. Chem. C 120 (2016) 9132–9147.
[64] G.T.K.K. Gunasooriya, A.P. van Bavel, H.P.C.E. Kuipers, M. Saeys, ACS Catal. 6 (2016) 3660–3664.
[65] X. Yu, X. Zhang, S. Wang, Appl. Surf. Sci. 353 (2015) 973–978.
[66] X. Yu, X. Zhang, Y. Meng, Y. Zhao, Y. Li, W. Xu, Z. Liu, Appl. Surf. Sci. 434 (2018) 464–472.
[67] M.T. Yu, L.L. Liu, Q. Wang, L.T. Jia, B. Hou, Y.B. Si, D.B. Li, Y. Zhao, Int. J. Hydrogen Energy 43 (2018) 5576–5590.
[68] Q. Wang, R.G. Zhang, L.T. Jia, B. Hou, D.B. Li, B.J. Wang, Int. J. Hydrogen Energy 41 (2016) 23022–23032.
[69] P. van Helden, J.A. van den Berg, C.J. Weststrate, ACS Catal. 2 (2012) 1097–1107.
[70] W.J. Luo, A. Asthagiri, J. Phys. Chem. C 118 (2014) 15274–15285.

[71] A.N. Pour, Z. Keyvanloo, M. Izadyar, S.M. Modaresi, Int. J. Hydrogen Energy 40 (2015) 7064–7071.
[72] I.M. Ciobica, R.A. van Santen, J. Phys. Chem. B 107 (2003) 3808–3812.
[73] C.J. Weststrate, P. van Helden, J. van de Loosdrecht, J.W. Niemantsverdriet, Surf. Sci. 648 (2016) 60–66.
[74] C.C. Liu, Y. He, L. Wei, Y.H. Zhang, Y.X. Zhao, J.P. Hong, S.F. Chen, L. Wang, J.L. Li, ACS Catal. 8 (2018) 1591–1600.
[75] Z. Zhao, W. Lu, R.O. Yang, H.J. Zhu, W.D. Dong, F.F. Sun, Z. Jiang, Y. Lyu, T. Liu, H. Du, Y.J. Ding, ACS Catal. 8 (2017) 228–241.
[76] B. Zeng, B. Hou, L.T. Jia, J.G. Wang, C.B. Chen, D.B. Li, Y.H. Sun, Catal. Sci. Technol. 3 (2013) 3250–3255.
[77] B. Zeng, B. Hou, L. Jia, J. Wang, C. Chen, Y. Sun, D. Li, ChemCatChem 5 (2013) 3794–3801.
[78] P. Senecal, S.D.M. Jacques, M. Di Michiel, S.A.J. Kimber, A. Vamvakeros, Y. Odarchenko, I. Lezcano-Gonzalez, J. Paterson, E. Ferguson, A.M. Beale, ACS Catal. 7 (2017) 2284–2293.
[79] P. van Helden, J.A. van den Berg, I.M. Ciobîcă, Catal. Sci. Technol. 2 (2012) 491–494.
[80] P. van Helden, I.M. Ciobîcă, R.L.J. Coetzer, Catal. Today 261 (2016) 48–59.
[81] J. Zheng, J. Cai, F. Jiang, Y.B. Xu, X.H. Liu, Catal. Sci. Technol. 7 (2017) 4736–4755.
[82] C.F. Huo, B.S. Wu, P. Gao, Y. Yang, Y.W. Li, H.J. Jiao, Angew. Chem. Int. Ed. 50 (2011) 7403–7406.